



CHALMERS
UNIVERSITY OF TECHNOLOGY

Graphene Film for Multifunctional Graphene-Based Thermal Interface Material with Bidirectional High Thermal Conductivity

Downloaded from: <https://research.chalmers.se>, 2026-03-10 22:28 UTC

Citation for the original published paper (version of record):

Guo, S., Wang, M., Wang, Y. et al (2025). Graphene Film for Multifunctional Graphene-Based Thermal Interface Material with Bidirectional High Thermal Conductivity. *Small Structures*, 6(7). <http://dx.doi.org/10.1002/sstr.202400652>

N.B. When citing this work, cite the original published paper.

Graphene Film for Multifunctional Graphene-Based Thermal Interface Material with Bidirectional High Thermal Conductivity

Sihua Guo, Minghe Wang, Yuanyuan Wang, Jin Chen, Kristoffer Harr, Lijie He, Yong Zhang,* Yan Zhang,* Bin Wei,* and Johan Liu*

Multifunctional and eco-friendly thermal interface materials with bidirectional thermal conductivity have become outstanding materials for solving the heat dissipation problem of electronic devices. The remarkable thermal and mechanical properties of graphene establish it as a promising material for thermal management. This study introduces an environmentally friendly strategy to construct an effective thermal conductive path by assembling and stacking recycled graphene strips (GS) under external mechanical force and using them as reinforcement to strengthen epoxy resin (EP) composites. By adjusting the loading of GS, a superior vertical thermal conductivity of 104.6 W mK^{-1} is achieved accompanied by a parallel thermal conductivity of 10.6 W mK^{-1} , representing enhancement of 614 and 61 times compared to that of the pure EP, respectively. The outstanding bidirectional thermal conductivity, along with ultralow thermal resistance, strong electromagnetic interference shielding, high-efficiency Joule heating, as well as excellent mechanical properties, offers a promising way to address the thermal management challenges of next-generation electronic devices.

1. Introduction

The continuous miniaturization and increased integration of electronic devices have led to increased heat dissipation in the equipment.^[1–4] Thermal interface materials (TIM), which are usually used to fill the gaps between heat sinks and heat-generating components, have received widespread attention.^[5–8] Owing to its remarkable thermal and mechanical properties, graphene is deemed to be the most promising candidate material for thermal management problems.^[9–12] The traditional solution is to mix


graphene and polymers. However, the random orientation of graphene and the high interfacial thermal resistance limit the thermal conductivity of the composite.^[13,14]

To achieve excellent thermal conductivity, constructing a horizontal conduction structure to fabricate the graphene-enhanced TIM is an effective strategy.^[15–19] Mani et al.^[20] presented graphene nanoplatelets/polyurethane (GnP/PU) films utilizing the solution casting approach, exhibiting a thermal conductivity of 10.68 and 0.46 W mK^{-1} in the parallel and vertical directions. Ruan et al.^[21] constructed NH_2 -reduced graphene oxide/polyimide (NH_2 -rGO/PI) films by blade coating, and corresponding composites were shown in-plane and through-plane thermal conductivity of 7.13 and 0.74 W mK^{-1} , respectively. In addition, other methods also have been proposed to construct horizontally aligned graphene structures.^[22,23] Although arranging graphene sheets into films can

effectively improve the parallel (in-plane) thermal conductivity of heat dissipation materials, it is relatively difficult to significantly increase their vertical (through-plane) thermal conductivity. However, TIM needs to have high bidirectional thermal conductivity in practical applications.^[24]

Therefore, various assembled graphene architectures have been constructed to improve the bidirectional thermal conductivity of the composites so that the inherent thermal performance of graphene can be extended to macroscopic graphene-enhanced TIM.^[25–29] Hu et al.^[30] reported 3D fluorinated boron nitride

S. Guo, M. Wang, Y. Zhang, Y. Zhang, B. Wei
School of Mechatronics Engineering and Automation
SMIT Center
Shanghai University
20 Chengzhong Rd., Shanghai 201800, P. R. China
E-mail: yongz@shu.edu.cn; yzhang@shu.edu.cn; bwei@shu.edu.cn

 The ORCID identification number(s) for the author(s) of this article can be found under <https://doi.org/10.1002/ssstr.202400652>.

© 2025 The Author(s). Small Structures published by Wiley-VCH GmbH. This is an open access article under the terms of the Creative Commons Attribution License, which permits use, distribution and reproduction in any medium, provided the original work is properly cited.

DOI: 10.1002/ssstr.202400652

Y. Wang, K. Harr, L. He
SHT Smart High-Tech AB
Arendals Allé 3, SE-418 79 Gothenburg, Sweden

J. Chen
Shanghai Ruixi New Materials High Tech Co. Ltd.
No 818, Chuhua North Road, Shanghai, P. R. China

J. Liu
Department of Microtechnology and Nanoscience
Electronics Materials and Systems Laboratory
Chalmers University of Technology
Kemivägen 9, SE 412 96 Gothenburg, Sweden
E-mail: jliu@chalmers.se

nanosheets (F-BNNS)/graphene oxide (GO)/polydimethylsiloxane (PDMS) composite prepared by bi-directional freezing assembly and vacuum-infiltrating method, with thermal conductivity of 3.28 and 0.8 W mK⁻¹ in through-plane and in-plane direction, respectively. Also, Li et al.^[31] demonstrated an all-graphitized graphene foam by directional-freezing graphene oxide hydrogels, freezing-drying and graphitization at 2800 °C for epoxy composites. Nevertheless, these methods are expensive and complex, lacking scalability and potential for industrialization. Meanwhile, the large number of pores inside the foam can increase interface phonon scattering, hindering heat dissipation.^[24] Therefore, developing low-cost, scalable TIMs with bidirectional high thermal conductivity remains a great challenge.

In this study, graphene strips/epoxy (GS/EP) composite with outstanding bidirectional thermal conductivity was fabricated by an environmentally friendly method, in which GS originated from the graphene film fragments created in the commercial mass production of graphene-enhanced TIM. Particularly, the raw materials used here were inexpensive, and the preparation process was simple without any modification steps. The directionally arranged graphene served as the primary heat transfer channel, guiding heat to be effectively transferred along the constructed framework, thereby reducing phonon scattering and interface thermal resistance. Meanwhile, the composite displays a spectrum of engaging multifunctional features, encompassing ultralow thermal resistance, strong electromagnetic interference (EMI) shielding, high-efficiency Joule heating, as well as impressive mechanical properties.

2. Experimental Section

2.1. Materials

Graphene film was provided by SHT Smart High-Tech AB. The structural characterization of graphene film is shown in Figure S1, Supporting Information. The graphene film was pretreated to the uniformly sized GS. EP and methyltetrahydrophthalic anhydride were supplied by Runxiang Chemical Co., Ltd., in which methyltetrahydrophthalic anhydride was used as the curing agent.

2.2. Preparation of GS/EP Composites

The preparation process of the GS/EP composite is shown in Figure 1. Specifically, EP was mixed with methyl tetrahydrophthalic anhydride, stirred for 1 h, and ultrasonically treated for 30 min. Subsequently, the mixture was placed in a vacuum oven at room temperature and evacuated for 30 min to remove bubbles. After that, the GS was mixed uniformly with the EP mixture. The GS impregnated with EP mixture was stacked layer by layer in a homemade mold, and a composite block was obtained by curing at 150 °C for 3 h under the action of mechanical external force. In the end, the composite block was cut along the vertical (Z-plane) and parallel (X–Y in-plane) directions to obtain GS/EP composite. By using the same amount of EP mixture and GS, composite blocks with different GS contents can be obtained by controlling the block height. The preparation method of the comparative composite was as follows: GS and EP mixture

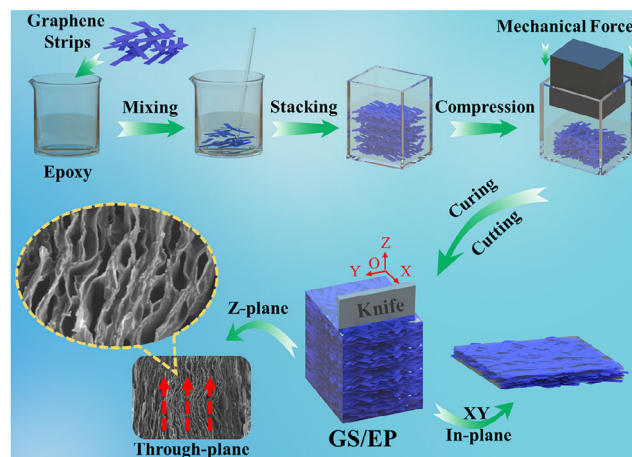


Figure 1. A schematic illustration of the manufacturing procedure for the GS/EP composites.

are mixed and then directly put into the mold. The remaining process is the same as the preparation method of the GS/EP composite, and a randomly distributed graphene strips/epoxy (RGS/EP) composite was obtained.

2.3. Characterization

X-ray photoelectron spectroscopy (XPS) (Thermo Scientific K-Alpha, USA) was performed to determine the elemental composition of graphene film. The crystal structure of graphene film was characterized via X-ray diffraction (XRD) (Rigaku Ultima IV, Japan). Raman spectra (Horiba LabRAM HR Evolution, Japan) were used to test the defect structure of graphene film. The cross-sectional morphology of the materials was obtained by scanning electron microscopy (SEM) (ZEISS GeminiSEM 300, Germany). The thermal conductivity of the composites was measured using an interfacial thermal resistance meter (Xiangke DRL-V, Xiangtan), which the schematic diagram (Figure S2) and test principle are shown in the SI. The calculation formula of thermal conductivity is^[32]

$$R = \frac{BLT}{K} \quad (1)$$

where R , BLT , and K are the thermal resistance, bond line thickness, and thermal conductivity of the composites, respectively. The mechanical performances of the composites were evaluated through an electronic universal testing machine (INSTRON 5982 CMT4104, America) at a strain rate of 1 mm min⁻¹. An infrared thermal imager (Fluke, Ti400, USA) was used to capture thermal images to obtain the surface temperature changes. The electromagnetic interference shielding effectiveness (EMI SE) of the composites in the X-band frequency range of 8.2 to 12.4 GHz was measured through the waveguide method using a vector network analyzer (Agilent E5071C, USA). The size of the sample is 22.9 mm × 10.2 mm × 1 mm. The scattering parameters S_{11} , S_{12} , S_{21} , and S_{22} can be directly obtained, and then the total EMI SE (SET), absorption loss (SEA), and reflection loss (SER) are calculated using the following formulas^[33]

$$R = |S_{11}|^2 \quad (2)$$

$$T = |S_{21}|^2 \quad (3)$$

$$A = 1 - R - T \quad (4)$$

$$SE_R = 10 \lg \left| \frac{1}{1-R} \right| \quad (5)$$

$$SE_A = 10 \lg \left| \frac{1-R}{T} \right| \quad (6)$$

$$SE_T = 10 \lg \left| \frac{1}{T} \right| = SE_A + SE_R \quad (7)$$

3. Results and Discussion

The GS/EP composite prepared using 2 mm × 12 mm GS not only has thermal properties close to those of composite prepared from high-quality graphene but also reduces costs and has an environmentally friendly concept. Therefore, this study selects 2 mm × 12 mm GS to prepare GS/EP composites (Figure S3). The thermal resistance of GS/EP composites with different GS content at 80 °C and different pressures were studied (Figure 2a). As the pressure increases, the thermal resistance gradually

decreases and tends to level off. Since the assembly pressure of electronic equipment is generally 40 psi, the thermal resistance at 40 psi was selected to obtain the thermal conductivity of the GS/EP composites. The thermal conductivities of GS/EP composites with different GS content were measured in the parallel (//) and bidirectional (⊥) directions. The GS/EP composites exhibit high bidirectional heat transfer capability. Notably, at a GS content of 63.5 wt%, the (⊥) and (//) thermal conductivity of GS/EP composite reached an impressive value of 104.6 and 10.6 W mK⁻¹, corresponding to 615 times and 61 times higher than that of pure EP, respectively. Nevertheless, the (⊥) and (//) thermal conductivities of the RGS/EP composite are ≈20.3 and 11.4 W mK⁻¹, respectively (Figure 2b). To account for the vertical thermal conductivity's escalation, Figure 2c,d illustrates the cross-sectional SEM images of GS/EP composites. The GS/EP composites exhibit a vertically stacked arrangement.

Additionally, there is a certain amount of bridging between the layers, ensuring that the GS/EP composites have bidirectional thermal conductivity. The graphene layers are arranged vertically, providing the direct heat conduction path from the hot end to the cold end and greatly enhancing the efficiency of heat transfer. On the contrary, the disordered structure of RGS/EP composites greatly hinders the effective transfer of heat.

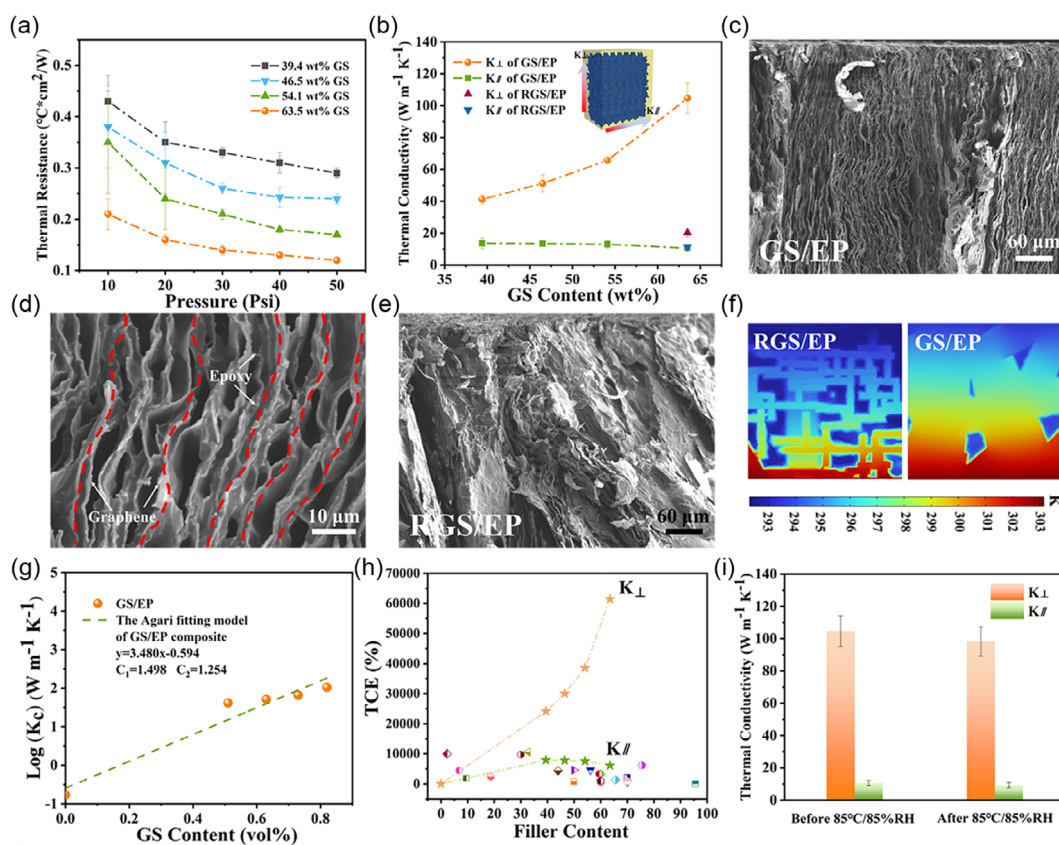


Figure 2. a) Thermal resistance of the GS/EP composite with various GS content at different pressures. b) The vertical (K_{\perp}) and parallel ($K_{//}$) thermal conductivity of the composites. Cross-sectional morphology of c,d) GS/EP (the red dashed line shows the direction of heat flow) and e) RGS/EP composite at 63.5 wt% GS content. f) Temperature distributions in RGS/EP and GS/EP composites simulated by finite element simulation. g) Agari model simulation of GS/EP composite. h) TCE of the GS/EP composites in the vertical and parallel direction with different GS contents and other composites reported previously. i) Thermal conductivity of GS/EP composite with 63.5 wt% GS content before and after the 85 °C/85%RH damp heat test.

Numerical simulations were carried out to study the heat transfer performance of the composites, as shown in Figure 2f. Two kinds of distributions of GS in EP, namely random in space (RGS/EP) and random in layers (GS/EP), have been considered in the finite element simulations. In the RGS/EP model, the GS were randomly distributed in 3D epoxy matrix. In the GS/EP model, the GS are generated with a random distribution in an epoxy layer, and then layers of the mixture are stacked so as to simulate the experimental preparation process. Temperature distributions of RGS/EP and GS/EP composites during the heat transfer process were obtained by transient simulation (for more modeling details, refer to the SI).

Meanwhile, the Agari model can effectively predict the thermal conductivity of composite with high filler content. The model equation is^[34]

$$\log K_c = V_f C_2 \log K_f + (1 - V_f) \log(C_1 K_m) \quad (8)$$

Here, K_c , K_f (200 W mK^{-1}), and K_m (0.17 W mK^{-1}) represent the thermal conductivity of the composites, GS and EP, respectively. V_f represents the volume fraction of GS. C_1 is the parameter for the influence of the filler on polymer matrix structure, and C_2 is the difficulty of predicting the formation of thermal conductive chains by fillers (the higher the C_2 , the easier it is to form thermal conductive chains). Thus, the C_1 and C_2 of the GS/EP composites can be calculated, where C_2 was 1.254, which was higher than the general value (0–1) (Figure 2g).^[35] This indicates that the directional graphene framework in GS/EP composites was more likely to form heat conduction channels, effectively promoting the conduction of phonons, and thereby improving the thermal conductivity of the composite.

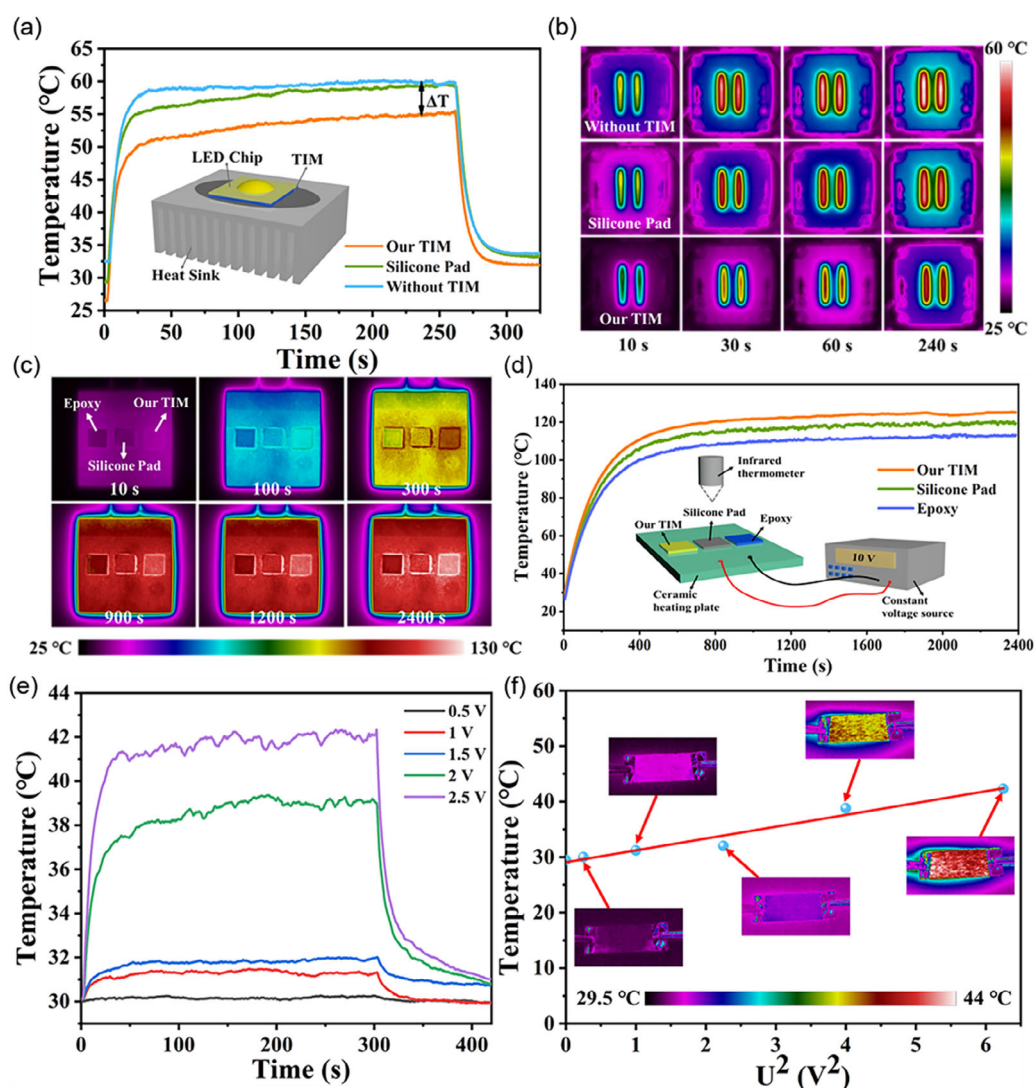


Figure 3. a) Temperature curves of the LED modules during the heating and subsequent natural cooling process, with an inset showing a schematic diagram of LED heat transfer application. b) Infrared thermal image of the LED modules taken using a thermal imager. c) Infrared images of epoxy, commercial silicone pad, and our TIM on the ceramic heating plate. d) Comparison of temperature rise of different samples in (c). e) Surface temperature of GS/EP composites as a function of time under various input voltages. f) Experimental data and linear fitting of temperature and U^2 .

Therefore, theoretical analysis further demonstrates the superiority of the oriented graphene framework in enhancing heat transfer in composites.

Figure 2h summarizes the thermal conductivity enhancement (TCE) of previously reported composites (more details in Table 1, Supporting Information). Among the reported composites, the GS/EP composites exhibited the highest TCE. After 720 h of 85 °C/85% relative humidity (RH) damp heat test, the thermal properties of GS/EP composites decreased slightly (Figure 2i). The reason is that the high temperature and high humidity environment destroyed the C=O bonds and O—C=O bonds in the GS/EP composites. The presence of C=O bonds and O—C=O bonds can enhance the interface bonding between graphene and epoxy, thereby improving the thermal conductivity of GS/EP composites. However, the destruction of these bonds leads to a decrease in the thermal conductivity of the GS/EP composites during the aging process (Figure S6).

Traditional heat sinks and TIMs play a vital role in electrical equipment cooling systems. The heat sink is responsible for transferring heat to the environment, while the TIM located between the electronic component and the heat sink is used to accelerate the heat transfer between the contact surfaces. Using TIMs with high through-plane thermal conductivity facilitates rapid heat dissipation.^[36] A proof-of-concept experiment was conducted to verify the device-cooling performance of the GS/EP composite through the integration and in situ characterizations of an light-emitting diode (LED) chip during its operation (Figure 3a). The commercial silicone pad ($4 \text{ W m}^{-1} \text{ K}^{-1}$) and GS/EP composites (63.5 wt% GS and $104.6 \text{ W m}^{-1} \text{ K}^{-1}$) were used as TIM between the heat sink and 20 W LED chip, respectively. The stable temperatures of LED chip without TIM, with commercial silicone pad and with GS/EP composite were 60, 59, and 55 °C, respectively. Moreover, the infrared thermal image vividly demonstrated the excellent heat dissipation ability of GS/EP composites after lighting up the LED chip (Figure 3b).

To more comprehensively illustrate the differences in thermal conductivity, pure EP, commercial silicone pad and GS/EP composites of the same size ($10 \text{ mm} \times 10 \text{ mm} \times 1 \text{ mm}$) were fixed

on a ceramic heating plate using thermal grease, and a voltage of 10 V was applied. After 2400 s, the surface temperature of GS/EP composites reached 125 °C, which is higher than that of EP (113 °C) and thermal pad (119 °C), as shown in Figure 3c,d. This is attributed to the excellent heat conduction performance given by the high-quality directional arrangement of graphene in GS/EP composites. Therefore, the GS/EP composite shows great potential to become a commercial TIM.

To overcome the negative impact of a low-temperature environment on the operational stability of electronics devices, it is necessary to develop materials with heating capabilities.^[37,38] The Joule heating behavior of the GS/EP composites was studied by applying different external voltages and recording the surface temperature changes over time using an infrared thermal imager. When the voltage increased from 0.5 to 2.5 V, the temperature increased from 30 to 42 °C (Figure 3e). Simultaneously, the relationship between the surface temperature and voltage of the GS/EP composite was investigated, revealing that the surface temperature had a linear relationship with U^2 , which was consistent with the Joule heating principle (Figure 3f).^[37,39]

To evaluate the cooling performance of our TIM in practical application, a desktop computer-based validation system was designed (Figure 4a).^[40] We fixed the GS/EP composite, thermal grease, and commercial TIM between the central processing unit (CPU) (Intel core i3 10100) and the cooling fan using spring screws, respectively. Professional software performs a full load test on the CPU and monitors its temperature changes. As the software runs, the CPU temperature rises rapidly and stabilizes after 360 s. Compared to the thermal grease and commercial TIM, the GS/EP composite significantly reduced the CPU temperature. At 360 s, the CPU temperature with GS/EP composite was 78 °C, which was notably lower than that of the commercial TIM (91 °C) and the thermal grease (87 °C) (Figure 4c). This result demonstrates that the GS/EP composite can effectively transfer heat from the CPU to the cooling fan, exhibiting excellent thermal conductivity. Thermal grease is commonly used as a TIM to conduct heat away from the CPU, but it has several disadvantages, such as the following: (1) Thermal grease can dry

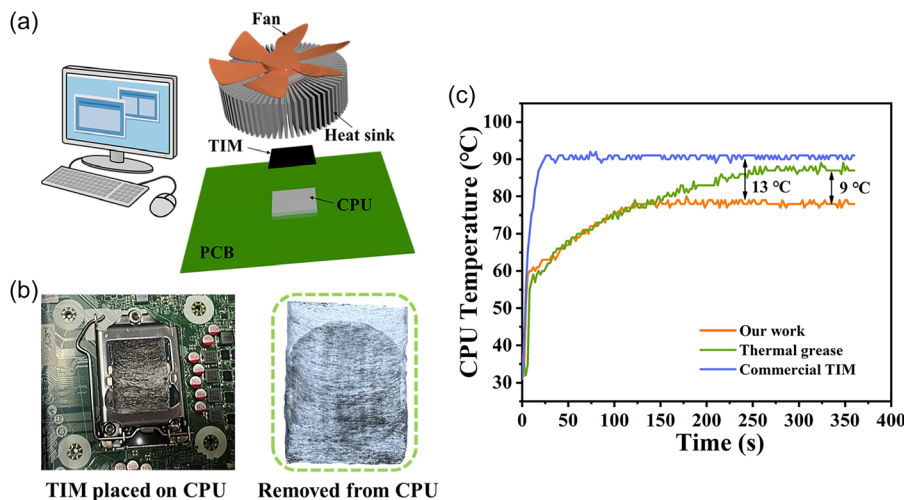


Figure 4. a) Schematic diagram of the CPU thermal management system. b) Schematic diagram of the experimental part, our TIM on the CPU and the TIM removed from the CPU. c) CPU core temperature variation with heating time.

out, harden, or evaporate over time, leading to a decline in thermal performance and requiring periodic replacement; (2) applying thermal grease requires precise control of thickness and uniformity; and (3) the grease may leak from the CPU to other components on the motherboard, making it difficult to clean. Figure 4b shows that our TIM remains unchanged before and after use, indicating its suitability for long-term use. Moreover, our TIM has high thermal conductivity, making it ideal for high-performance or long-term cooling applications.

TIM must have good mechanical properties to meet the requirements of practical applications and prevent cracking during the packaging process. As the GS content decreases from 63.5 to 39.4 wt%, the tensile strength of the GS/EP composites increases from 0.105 to 0.139 MPa (Figure 5a). Meanwhile, the

compression strength of GS/EP gradually increases, and no yield fracture occurs under 80% compression strain, indicating its excellent compression resistance. Among them, the compression strength of the 63.5 wt% GS/EP composite at 50% compressive strain was 14.29 MPa (Figure 5c). The increase in EP content helps to encapsulate GS and effectively fill the microdefects and pores in the composite. By reducing these micro defects, the overall strength of the composite is improved. At the same time, after the 85 °C/85%RH damp heat test, the mechanical properties of the GS/EP composite decreased slightly (Figure 5b), which was caused by the decrease in the interfacial bonding strength between graphene and epoxy.

Electromagnetic shielding materials play a crucial role in maintaining the stable operation of electrical products and

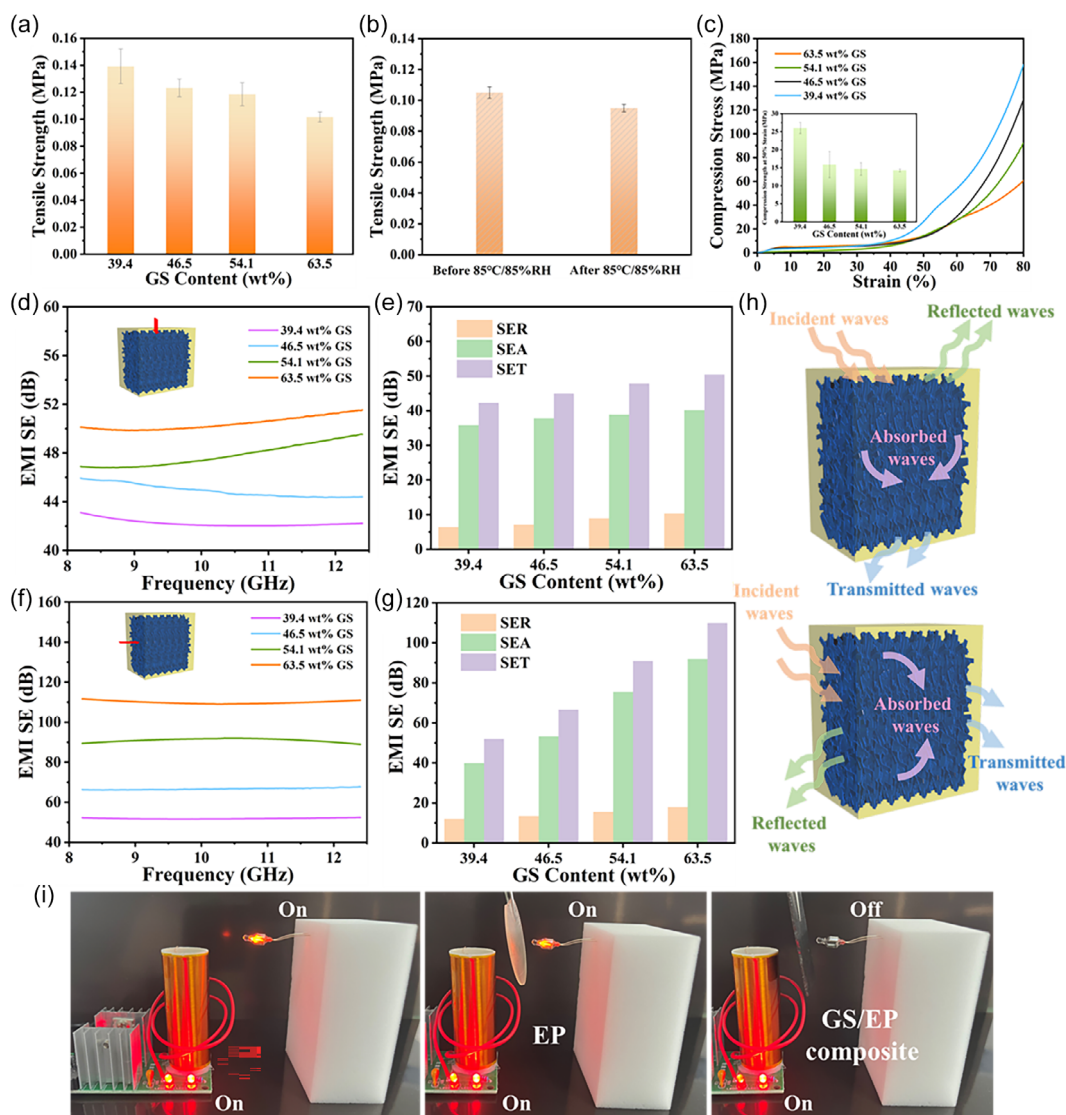


Figure 5. a) Tensile strength of the GS/EP composite with different GS content. b) Tensile strength of the GS/EP composite before and after the 85 °C/85%RH damp heat test. c) Compression stress–strain curves of the GS/EP composite at different GS content. And compression strength of the GS/EP composite at 50 % compression. EMI SE of GS/EP composite d,e) along the graphene direction f,g) perpendicular to the graphene direction. h) Illustration of EMI shielding mechanism for GS/EP composite. i) The practical application of the EMI shielding effect of the GS/EP composite after being put into a Tesla coil system.

communication base stations.^[41–43] The EMI shielding performance of GS/EP composites in the X-band (8.2 to 12.4 GHz) was studied, and the EMI SE of GS/EP composites along and perpendicular to the graphene directions is described in Figure 5d–g, showing a significant increase in EMI SE with increasing GS content. Specifically, when the GS content is 63.5 wt%, the EMI SE of the GS/EP composites along and perpendicular to the graphene directions reaches 50 and 110 dB, respectively. It is worth noting that the best thermal conductivity of GS/EP composites is along the direction of graphene, so this direction's GS/EP composites and pure EP were placed into a Tesla coil system. As shown in Figure 5i, the lamp goes out when the GS/EP composite is placed in the Tesla coil system, while the lamp of the EP system keeps glowing, indicating that the GS/EP composite has a significant shielding ability against electromagnetic waves (EMWs) in practical application. Figure 5h shows the attenuation mechanism of EMWs in EMI shielding of GS/EP composites. When EMWs propagate in different media, they encounter different electromagnetic impedances. Therefore, when EMWs enter the conductive composite from the air, part of the EMWs will be reflected due to the impedance mismatch between the two media.^[44–46] The remaining EMWs pass through the interconnected graphene framework. When EMWs are incident perpendicularly to the graphene framework, the graphene induces the generation of dipoles, accompanied by energy dissipation as well as multiple internal reflections and scattering, thereby enhancing the absorption of EMWs and effectively preventing their penetration.^[37,47] However, when EMWs are incident parallel to the graphene framework, part of the EMWs penetrate the EP molecules between the graphene layers, resulting in a decrease in EMI SE in this direction.^[48]

4. Conclusions

In summary, a multifunctional GS/EP composite with bidirectional thermal conductivity was prepared by an environmentally friendly stacking arrangement method. The vertical thermal conductivity of the composite reached 104.6 W mK^{-1} while maintaining an excellent parallel thermal conductivity of 10.6 W mK^{-1} . The superior bidirectional thermal conductivity was owing to the thermal transport channel constructed by assembling stacked graphene, which can make the heat transfer more efficient. The excellent thermal performance of the composite also was verified through practical applications. The GS/EP composite not only effectively reduces the core temperature of the computer CPU but also lowers the surface temperature of the LED chip and exhibits multifunctional properties such as the Joule heating effect and electromagnetic shielding. Importantly, this work provides a potential method for preparing commercial TIMs with bidirectional thermal conductivity to address the thermal management issues in next-generation electronic devices.

Supporting Information

Supporting Information is available from the Wiley Online Library or from the author.

Acknowledgements

The authors acknowledge the financial support from the Vinnova Siografen under the contract no. 2022-03831 as well as from the Production Area of Advance at Chalmers University of Technology, Sweden, and the financial support from the Shanghai Science and Technology Commission under the contract no. 22501100300. They also acknowledge the financial support from the Natural Science Foundation of Shanghai (no: 23ZR1424000). S.G. and M.W. contributed equally to this work.

Conflict of Interest

The authors declare no conflict of interest.

Author Contributions

Sihua Guo: methodology (lead) and writing—original draft (lead). **Minghe Wang:** methodology (equal). **Yuanyuan Wang:** resources (supporting). **Jin Chen:** resources (supporting). **Kristoffer Harr:** resources (supporting). **Lijie He:** resources (supporting). **Yong Zhang:** writing—review and editing (lead). **Yan Zhang:** methodology (equal) and resources (equal). **Bin Wei:** supervision (lead). **Johan Liu:** resources (lead); supervision (lead); and writing—review and editing (lead).

Data Availability Statement

Author elects to not share data.

Keywords

bidirectional high thermal conductivity, epoxy composites, light-emitting diode, recycled graphene strips, thermal interface materials

Received: December 11, 2024

Revised: April 17, 2025

Published online: June 9, 2025

- [1] S. Guo, S. Chen, A. Nkansah, A. Zehri, M. Murugesan, Y. Zhang, J. Liu, *2D Mater.* **2022**, *10*, 014002.
- [2] Y. Fan, Z. Wang, X. Guo, S. Yang, H. Jia, Z. Tao, J. Liu, *Diam. Relat. Mater.* **2024**, *143*.
- [3] Z. Ma, J. Wang, Z. Hao, J. Dai, X. Zhu, H. Zheng, Z. Lu, *Adv. Funct. Mater.* **2024**, *2412534*.
- [4] H. Zhang, Q. He, H. Yu, M. Qin, Y. Feng, W. Feng, *ACS Nano.* **2024**, *18*, 21399.
- [5] J. Jin, Y. Su, J. Guo, Z. Zhang, B. Peng, M. Chen, L. Wu, *Compos. Part B-Eng.* **2024**, *286*, 111780.
- [6] Z. Zhang, R. Yang, Y. Wang, K. Xu, W. Dai, J. Zhang, Y. Yu, *J. Mater. Chem. A* **2024**, *12*, 24428.
- [7] Z. G. Wang, Y. Huo, H. F. Nan, G. Zhang, J. Gao, L. Xu, Z. M. Li, *ACS Appl. Mater. Interfaces.* **2024**, *16*, 48386.
- [8] H. Yu, Y. Feng, C. Chen, Z. Zhang, Y. Cai, M. Qin, W. Feng, *Carbon.* **2021**, *179*, 348.
- [9] S. Guo, J. Chen, Y. Zhang, J. Liu, *Nanomaterials.* **2021**, *11*, 2539.
- [10] Y. Tong, X. Wang, X. Wang, Y. Wang, Y. Guo, F. Sun, Y. Li, *J. Alloy. Compd.* **2024**, *1003*, 175654.
- [11] W. Huang, Z. Wang, H. Zhou, Z. Yu, Z. Hao, Y. Gao, J. Cai, *Appl. Therm. Eng.* **2024**, *246*, 122958.

- [12] H. Yu, C. Chen, J. Sun, H. Zhang, Y. Feng, M. Qin, W. Feng, *Nanomicro Lett.* **2022**, *14*, 135.
- [13] G. Zhang, S. Xue, F. Chen, Q. Fu, *Compos. Sci. Technol.* **2023**, *231*, 109784.
- [14] H. Yu, Y. Feng, C. Chen, H. Zhang, L. Peng, M. Qin, W. Feng, *Adv. Sci.* **2022**, *9*, e2201331.
- [15] X. Wu, H. Li, K. Cheng, H. Qiu, J. Yang, *Nanoscale.* **2019**, *11*, 8219.
- [16] H.-C. Yuan, C.-Y. Lee, N.-H. Tai, *Compos. Sci. Technol.* **2018**, *167*, 313.
- [17] Y. Wang, X. Zhang, X. Ding, Y. Li, P. Zhang, M. Shu, X. Tian, *Compos. Sci. Technol.* **2021**, *205*, 108693.
- [18] M. Yan, X. Chen, Y. Xu, Y. Pan, J. Li, J. Li, J. He, *Compos. Commun.* **2023**, *37*, 101428.
- [19] Y. C. Soong, C. W. Chiu, *J. Colloid Interf. Sci.* **2021**, *599*, 611.
- [20] D. Mani, M. C. Vu, C.-S. Lim, J.-B. Kim, T.-H. Jeong, J.-H. Kim, S.-R. Kim, *Carbon.* **2023**, *201*, 568.
- [21] K. Ruan, Y. Guo, C. Lu, X. Shi, T. Ma, Y. Zhang, J. Gu, *Research* **2021**, *2021*, 8438614.
- [22] G. Li, X. Tian, X. Xu, C. Zhou, J. Wu, Q. Li, Y. Li, *Compos. Sci. Technol.* **2017**, *138*, 179.
- [23] S. Guo, R. Zheng, J. Jiang, J. Yu, K. Dai, C. Yan, *Compos. Part B-Eng.* **2019**, *178*, 107489.
- [24] Y. Zhang, W. Wang, F. Zhang, L. Huang, K. Dai, C. Li, Q. Zheng, *Carbon.* **2022**, *189*, 265.
- [25] Z. Liu, Y. Chen, Y. Li, W. Dai, Q. Yan, F. E. Alam, J. Yu, *Nanoscale* **2019**, *11*, 17600.
- [26] P. Sun, H. Yang, W. Sima, T. Yuan, M. Yang, X. Tang, S. Huang, *Compos. Commun.* **2024**, 102162.
- [27] T. Yang, Z. Jiang, H. Han, X. Cai, Y. Liu, X. Zhang, J. Hu, *Compos. Part B-Eng.* **2021**, *205*, 108509.
- [28] F. An, X. Li, P. Min, P. Liu, Z. G. Jiang, Z. Z. Yu, *ACS Appl. Mater. Interfaces* **2018**, *10*, 17383.
- [29] Z. Wang, Y. Cao, D. Pan, S. Hu, *Polymers* **2020**, *12*, 1121.
- [30] T. Huang, Y. Li, M. Chen, L. Wu, *Compos. Sci. Technol.* **2020**, *198*, 108322.
- [31] X.-H. Li, P. Liu, X. Li, F. An, P. Min, K.-N. Liao, Z.-Z. Yu, *Carbon* **2018**, *140*, 624.
- [32] J. Hansson, T. M. J. Nilsson, L. Ye, J. Liu, *Int. Mater. Rev.* **2017**, *63*, 22.
- [33] J. Li, Y. Wang, T.-N. Yue, Y.-N. Gao, Y.-D. Shi, J.-B. Shen, M. Wang, *Compos. Sci. Technol.* **2021**, *206*, 108681.
- [34] Y. Agari, A. Ueda, S. Nagai, *J. Appl. Polym. Sci.* **1993**, *49*, 625.
- [35] J. Chen, X. Huang, Y. Zhu, P. Jiang, *Adv. Funct. Mater.* **2016**, *27*, 1604754.
- [36] F. Zhang, D. Ren, Y. Zhang, L. Huang, Y. Sun, W. Wang, Q. Zheng, *Chem. Eng. J.* **2022**, *431*, 134102.
- [37] D. Yin, H. Xiu, S. Wang, Y. Pan, N. Li, R. Cheng, J. Li, *Nano Res.* **2024**, *17*, 4544.
- [38] J. Li, W. Zhang, L. Yang, S. Yin, *Compos. Commun.* **2023**, *38*, 101476.
- [39] Y. Zhang, Z. Ma, K. Ruan, J. Gu, *Nano Res.* **2022**, *15*, 5601.
- [40] B.-W. Wang, H. Zhang, Q.-X. He, H.-T. Yu, M.-M. Qin, W. Feng, *Chinese J. Polym. Sci.* **2024**, *42*, 1002.
- [41] Z. Nan, W. Wei, Z. Lin, J. Ouyang, J. Chang, Y. Hao, *Mat. Sci. Eng. R.* **2024**, *160*, 100823.
- [42] J. Liu, M.-Y. Yu, Z.-Z. Yu, V. Nicolosi, *Mater. Today.* **2023**, *66*, 245.
- [43] X. Hou, X.-R. Feng, K. Jiang, Y.-C. Zheng, J.-T. Liu, M. Wang, *J. Mater. Sci. Technol.* **2024**, *186*, 256.
- [44] H. Dong, Z. Liu, J. Guo, S. Lv, H. Huang, X. Jiang, *Chem. Eng. J.* **2024**, *490*, 151620.
- [45] Y. Zhang, K. Ruan, X. Shi, H. Qiu, Y. Pan, Y. Yan, J. Gu, *Carbon.* **2021**, *175*, 271.
- [46] K. Gong, Y. Peng, A. Liu, S. Qi, H. Qiu, *Compos. Part A-Appl. S.* **2024**, *176*, 107857.
- [47] J. Xu, R. Li, S. Ji, B. Zhao, T. Cui, X. Tan, T. L. Ren, A. C. S. Nano. **2021**, *15*, 8907-8918.
- [48] C. Wu, L. Zeng, G. Chang, Y. Zhou, K. Yan, L. Xie, Q. Zheng, *Adv. Compos. Hybrid Ma.* **2023**, *6*, 31.